DOI: 10.13009/EUCASS2023-474
Aerospace Europe Conference 2023 – 10TH EUCASS – 9TH CEAS

Experimental study of pulsed triggering oscillation in T-burner

*Ruyao Wang *, Junwei LI *†, Deyou Wang *, Jiajin Zeng *and Ningfei Wang **
** School of Aerospace Engineering, Beijing Institute of Technology*
No. 5, South Street, Zhongguancun, Haidian District, Beijing, China
ruyaowang@163.com – davidlee78@gmail.com
† Corresponding Author

Abstract
The aim of this work is to determine the validity of the pulse on measuring pressure coupling response by using T-burner. A pulse ignition system based on T-burner was designed to measure the characteristics of pressure oscillation. The oscillation waveform, amplitude, frequency, propagation velocities and attenuation constant of pulse wave were explored by changing pulse charge and chamber pressure. The results show that the propagation velocities of pulse wave decreased to the local speed of sound after 2-3 periods, which indicated that there was a waveform transforming process in the T-burner. Besides, the effect of waveform conversion under different conditions needs to be considered during the measurement of the pressure coupling response function.

1. Introduction

Pressure coupling response function is a typical characteristic parameter for predicting combustion stability of solid rocket motors [1]. Due to its simple design and ease of use, T-burner has become one of the most commonly used experimental devices for measuring response functions. However, the addition of alumina powder in high energy solid propellants makes it difficult to excite self-sustaining oscillation within a conventional T-burner [2,3]. Therefore, researchers have improved the T-burner with additional pulsers to trigger pressure oscillations [4,5].
Kaplan [6] modified an available T-burner setup to obtain the response of the solid propellant at different excitation frequencies by altering the chamber length. Various frequencies and mean pressure values were tested, and the effect of the burning surface on pressure fluctuations was also investigated by altering the configuration of the propellant. Gallier [7,8] developed a velocity-coupled T-burner to assess the driving role of aluminium combustion. The pulser was located inside the T-burner to produce acoustic pressure oscillation. This work illustrates that the instability arises due to a thermoacoustic coupling between pressure waves and unsteady heat release from aluminium combustion, and provides a detailed understanding of aluminium combustion effects on stability.
However, most researches have mainly focused on the unstable phenomena after pulse triggering, while neglecting the characteristics of the pulse signal. Since the excitation characteristics have received less attention, the pulse charge and period selection criteria used in the measurements are not uniform. Therefore, it is difficult to provide a standard guideline for data processing, which leads to great uncertainty in the results of pressure coupling response measurements using pulsed T-burner. In order to fill the gap in pulse triggering studies, the experimental study was carried out to investigate the characteristics of the pressure oscillation after a pulse. The aim of this work is to determine the validity of the pulse on measuring pressure coupling response by using T-burner. The oscillation waveform, amplitude, frequency, propagation velocities and attenuation constant of pulse wave were investigated under different pulse charge and chamber pressure respectively. This work can help to provide the basic understanding of combustion instability.

2. Experimental setup and methods

2.1 Experimental setup

Figure 1 shows a schematic of the experimental T-burner system. The experimental set-up consisted of four parts: T-burner, pulser, ignition control system and data acquisition system. The T-burner was designed in a segmented

DOI: 10.13009/EUCASS2023-474

configuration consisting of the burner body, external combustion chamber and nozzle. The effective length of the T-burner was 3.154 m, the wall thickness was 0.01 m and the internal diameter was 0.1 m. To record the pressure signals at different positions, five pressure sensors were located at equal intervals on the wall of the burner at positions of 0L, 1/4L,1/2L, 3/4L, and L, numbered 1# to 5# respectively.

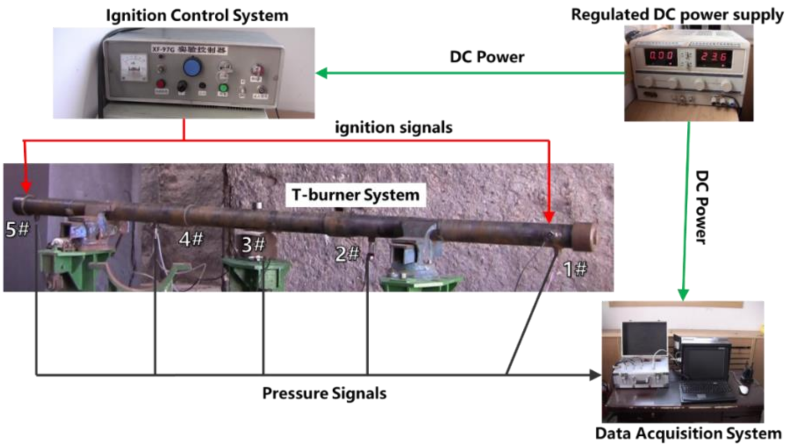

Figure 1: Schematic of the experimental T-burner system

The structure of the pulser was shown in Figure 2. The circular shell was made of stainless steel and had an internal insulating layer to prevent the electrical heating wire from short-circuiting when in contact with the shell. The black powder was placed at the bottom of the sealed end of the pulser, while the closed end of the U-shaped heating wire was buried in the black powder and the open end extended approximately 1 cm out of the pulser to connect with the ignition system. The pulser was filled with insulation to prevent transient short circuits of the heating wire, and the filler also served to seal the pulser. The DC power supply energized the electric ignitor, which rapidly heated the electric heating wire and ignited the black powder.

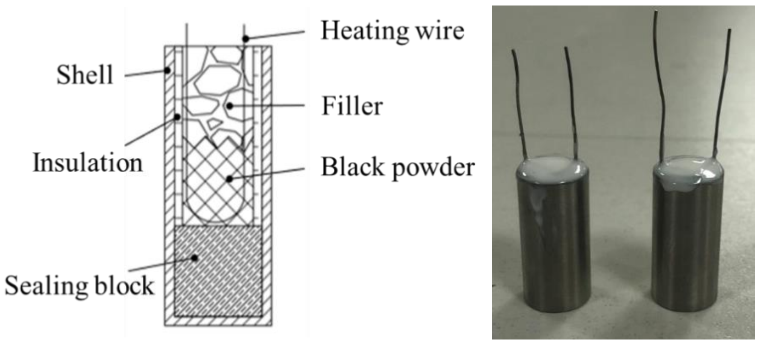

Figure 2: Schematic of the pulser

The ignition control system used the DC power supply, which model was Aim-TTi MX180TP with continuously adjustable output voltage from 0 V to 60 V and a maximum output power of 378 W. In the experiment, a voltage of 30 V was applied directly to achieve rapid ignition of the pulser. The data acquisition system consisted of pressure sensors, dynamic signal analyser and industrial control computer. The model of the pressure sensor was CYG4100 with a range of 0~4 MPa manufactured by Xi'an Jiecheng Co. Ltd. The supply voltage of the sensors was ±12 DCV, provided by a DC power supply, and the output signal of the sensors was 0~10 V with an accuracy of 0.25% FS. The model of the dynamic signal analyser was DH5922D produced by Jiangsu Donghua Testing Co. Ltd. The analyser had independent 24-bit A/D double-ended input connections for each channel, with a maximum continuous sampling rate of 256 kHz/channel and a range of ±100 mV to ±10 V, which can meet the sampling requirements for pulse testing.
The pulser, which was located inside the T-burner, was near the end of the chamber. The ignition control system sent an ignition signal to the pulser, then the black powder in pulser burnt quickly to form a pressure pulse. Due to the special structure of the T-burner, the pressure pulse wave propagated and reflected in chamber, then triggered the pressure oscillation. The pressure oscillation was monitored and recorded by the data Acquisition System. Two

DOI: 10.13009/EUCASS2023-474

groups of tests were carried out by changing powder charge and chamber pressure respectively, as shown in Table 1. In order to investigate the influence of pulse charge on the characteristic of pressure oscillation, powder charge was changed from 0.1g to 0.4g in tests 1-4. Besides, we increased the chamber pressure from 0 MPa to 2 MPa in tests 5-7. The pressure data was analysed based on Fast Fourier transform (FFT).

Table 1: Pulse-triggered experimental conditions

No.	**Pulse charge/g**	**Chamber pressure/MPa**	**Temperature/K**	**Diameter of T-burner /m**	**Length of T-burner /m**
R1~R4	0.1-0.4	0	273	0.12	3.154
R5~R7	0.4	0/1/2			

2.2 Data processing methods

The pressure oscillations in the T-burner are developed from the compression waves generated by a pulse. After the pulse excitation, the compression wave propagates to the wall of the chamber and then reflects, eventually superimposes to form pressure oscillations, as shown in Figure 3.

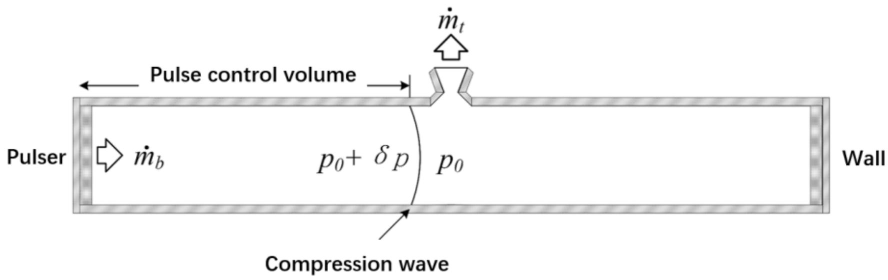

Figure 3: Developing process of the pulse wave in T-burner

Therefore, the propagation velocity of pulse can be calculated based on the time difference between the transmission of the pulse wave to each pressure sensor. It can be given by:

$$v_{\text{pulse}} = \frac{(n+1)L}{4(t_{\text{sensor}X} - t_{\text{sensor}Y})} \tag{1}$$

Where, v_{pulse} is the propagation velocity of the pulse, $t_{\text{sensor}X}$ is the effective time of the selected pulse front wave propagating to sensor X, $t_{\text{sensor}Y}$ is the effective time of the pulse front wave propagating to sensor Y, L is the length of the T-burner, n is the number of sensors between sensor X and sensor Y. According to the calculation, it is found that the propagation process of the pulse wave in the T-burner is not a uniform motion, but an accelerated motion. Therefore, the propagation velocity of the pulse is replaced by the average velocity of half a period of travel, which can reduce the amount of data processing and also facilitate comparison of data. Finally, in this paper, the pulse propagation velocity is calculated by using the results measured by the sensors on both sides of the T-burner:

$$v_{\text{pulse}} = \frac{L}{t_{\text{sensor5}} - t_{\text{sensor1}}} \tag{2}$$

DOI: 10.13009/EUCASS2023-474

2.3 The frequencies of acoustic modes

The acoustic waves are reflected and superimposed inside the T-burner to form acoustic modes. In this study, based on Rayleigh's criterion [9], the pulser is located at the pressure antinode / velocity node, which provides maximum gain for the acoustic oscillation system. In addition, the nozzle is located at the pressure node / velocity antinode, where the gas exhaust direction is perpendicular to the direction of longitudinal wave motion, resulting in minimal loss of the acoustic energy. Therefore, the T-burner can be simplified to a cylindrical acoustic cavity [10,11], and the frequencies of acoustic modes can be quickly estimated based on theoretical formulas:

$$f = \frac{\bar{a}}{2\pi}\sqrt{\left(\frac{k_{m,n}}{R_c}\right)^2 + \left(\frac{n_x \pi}{L_c}\right)^2} \tag{3}$$

Where, f is the frequency, $\bar{a}$ is the average speed of sound in T-burner. k is the complex wave number, the subscripts m, n represent the order of the purely tangential and radial modes respectively, R_c is the radius of the acoustic cavity, L_c is the length of the acoustic cavity.

3. Results and discussion

3.1 The characteristic of the pulse on pressure oscillation

Figure 4 shows the pressure signals measured by different sensors in T-burner chamber. The pulse charge was 0.1g, which represented the R1 condition listed in Table 1. It can be seen that the pressure in the chamber increases abruptly after the pulse triggering, followed by the gradual decay. The middle sensor $3^{\#}$ appears to have dominant harmonics at twice the frequency and half the amplitude compared to other sensors which are located at the ends. This is due to the fact that the pressure wave passes through the middle position twice in each oscillation period. As the total acoustic energy is conserved, the energy level or amplitude at the middle position is half the amplitudes at the ends of the T-burner.

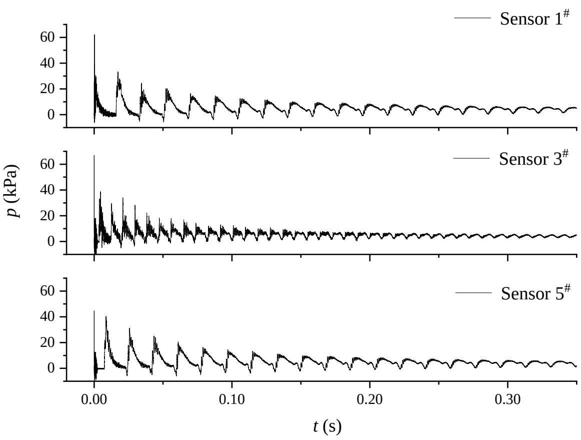

(a) Pressure-time curve

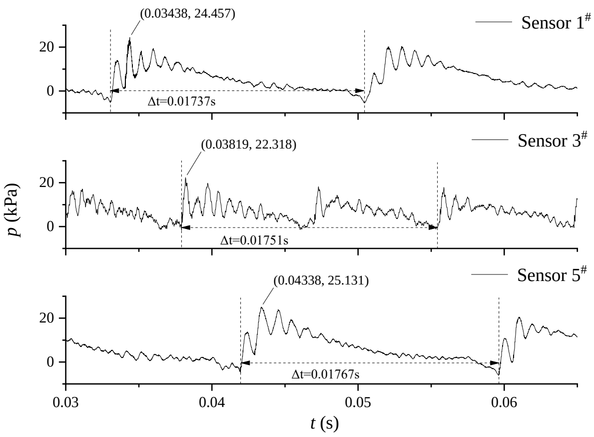

(b) Detail of the pressure-time curve

Figure 4: Pressure signals measured by the different sensors

Furthermore, the waveforms reveal that the pulse-triggered pressure oscillations are not simply first-order signals, but higher-order signals. Therefore, both longitudinal and transverse modes of oscillation in the chamber are analysed. Figure 5 shows the FFT results of the pressure signals in the time range of 0 to 0.5 s. It can be seen that there are several amplitude peaks in the range of frequencies below 600 Hz in Figure 5(a). The frequencies of the peaks are compared with the theoretical acoustic mode frequencies in Table 2. The results show that the experimental frequencies are in good agreement with the theoretical frequencies, indicating the presence of longitudinal oscillation modes formed by the pulse wave.

DOI: 10.13009/EUCASS2023-474

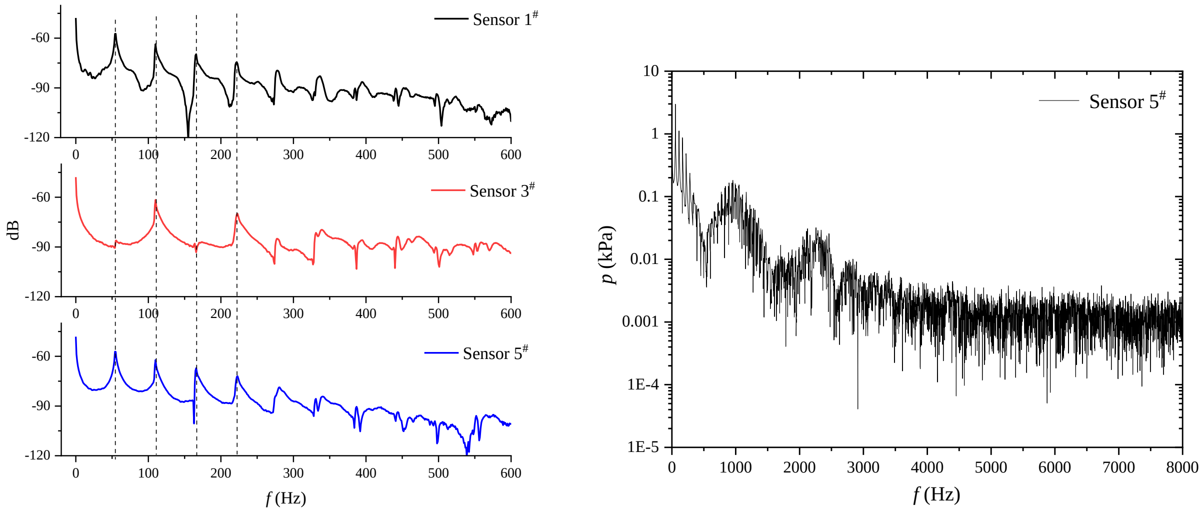

(a) 0-600Hz (b) 0-8000Hz

Figure 5: FFT results of the pressure oscillation

Table 2: Compression between the experimental frequencies with the theoretical longitudinal frequencies

Frequency/Hz	**1st order**	**2nd order**	**3rd order**	**4th order**
Theoretical	55.04	110.08	165.12	220.17
Sensor 1#	54.02	110.03	166.05	222.07
Sensor 3#	-	110.04	-	222.07
Sensor 5#	54.01	110.02	166.03	222.04

The FFT results at a higher frequency range were also analysed using the data from sensor 5#. Figure 5 (b) shows that there are peaks of amplitude in the high frequency range of the amplitude-frequency curve at 953.95Hz, 2123.75Hz, 2835.71Hz and 3402.44Hz respectively. In order to determine the type of oscillation, the theoretical frequencies of the tangential/radial modes are calculated to compare with the experimental results, as shown in Table 3. The results show that there is a coincidence between the experimental frequencies and the 1st / 2nd order frequencies of tangential modes, which indicates the possible existence of tangential oscillations. This conjecture will be further verified in subsequent experiments.

Table 3: Theoretical frequencies of transverse modes

Tangential/Radial	**0**	**1st order**	**2nd order**	**3rd order**
0	0	4235.866	7753.023	11242.4
1st order	**2034.604**	5892.02	9423.065	12936.75
2nd order	**3374.804**	7412.765	11016.72	14554.71
3rd order	4642.092	8857.126	12537.47	16120.59

The decay of the pressure oscillation was also studied. As shown in Figure 5, the pressure oscillations decay continuously as the number of periods increases during propagation. This is due to the presence of cavity damping and structural damping within the T-burner, resulting in the loss of acoustic energy. From the measured data, the attenuation constant of the pressure oscillations can be obtained, which represents the damping characteristics of the

DOI: 10.13009/EUCASS2023-474

T-burner under the corresponding operating conditions. The calculation of the attenuation constant is shown in Figure 6. The fluctuation pressure p' is obtained by subtracting the pressure data from the average pressure. The attenuation constant can be obtained by plotting the peak-to-peak amplitude–time curve of p' in a logarithmic time coordinate system. Obviously, the scatter points can be fitted to a straight line whose slope is the attenuation constant. The results of the attenuation constants measured by the three sensors in the condition R1 are shown in Table 4. It can be found that there is no significant difference between the attenuation constants measured at different positions.

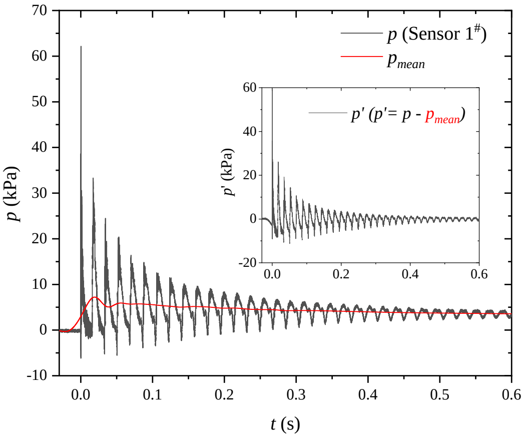

(a) The fluctuation pressure p'

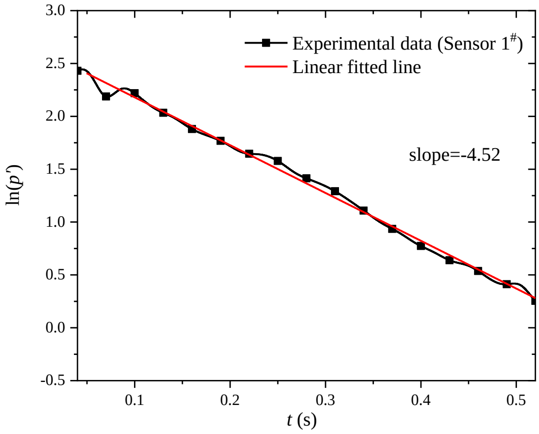

(b) The result of attenuation constant

Figure 6: The calculation principle of the attenuation constant

Table 4: The results of the attenuation constants

No. of sensor	The attenuation constant
1#	-4.52
3#	-4.47
5#	-4.80

According to Figure 4(b), there are time differences between the signals measured by the different sensors. The signal measured by the sensor located further away from the pulser lags behind that of the previous sensor. Therefore, according to the definition in section 2.2, the propagation velocities of the pulse with different periods were calculated, as shown in Figure 7. Where a period is defined as the time taken for the pulse wave to propagate from the pulser to the far wall and back to the pulser.

Figure 7 shows that the propagation velocities of the pulse are not close to the local velocity of sound initially, but has a much larger value and gradually decreases to near the theoretical velocity of sound after 2-3 periods. This suggests that the standing wave assumption widely used in traditional theory of combustion instability is not always valid. There is a conversion process in pulsed waveform from travelling waves to standing waves, which takes several periods. This is the reason for the great uncertainty in the results of pressure coupling response measurements using pulsed T-burners, as the typical traveling wave state present in the combustion chamber is not usually taken into account in data processing for the test results at present.

DOI: 10.13009/EUCASS2023-474

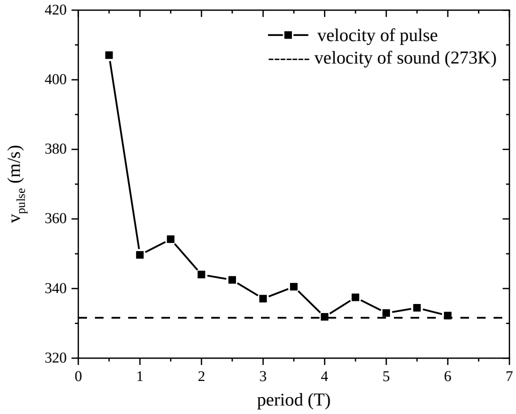

Figure 7: Propagation velocities of the pulse with different periods

3.2 The effects of the pulse charge on pressure oscillation

In order to investigate the effect of the pulse charge on the pressure oscillation characteristics, the pulse charge was changed from 0.1g to 0.4g in test 1-4. To avoid interference from the pulser bursting process on the results, the data measured by sensor $5^{\#}$ were selected in the following analysis. We defined δp as the amplitude of the first pulse and $\delta p/\delta t$ as the increase rate of the pressure to compare the variation pattern under different conditions. Figure 8(a) shows the pressure oscillation curves with different pulse charge, and the amplitude of the first pulse δp and the increase rate of the pressure $\delta p/\delta t$ are plotted in Figure 8(b). It can be seen that as the pulse charge mass increases, δp and $\delta p/\delta t$ rise rapidly, while the frequency of oscillation in the burner does not change significantly.

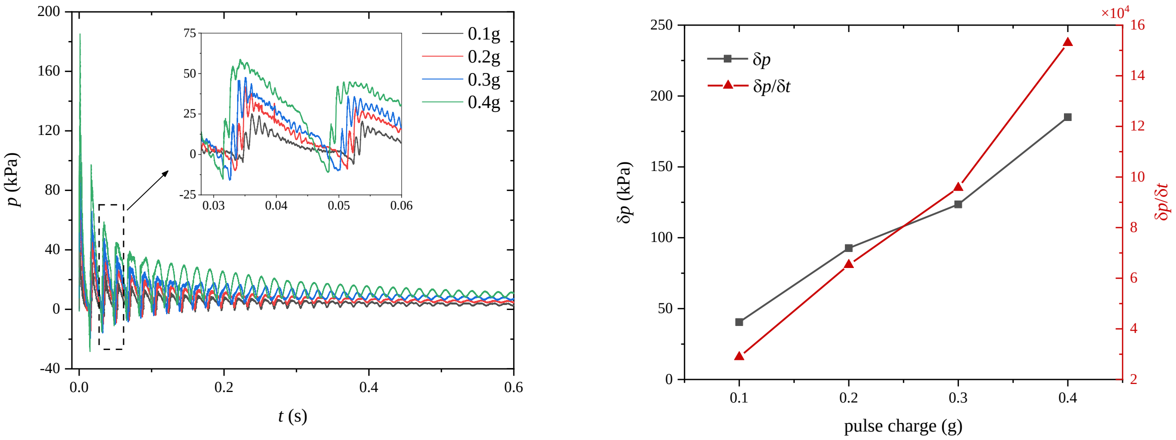

(a) The pressure oscillation curves (b) δp and $\delta p/\delta t$ with different pulse charge

Figure 8: The pressure signals under different pulse charge

FFT analyses were carried out on the pressure signals in the time range of 0 to 0.5 s to obtain the amplitude-frequency characteristics of the longitudinal oscillation at different pulse charges, as shown in Figure 9. The results show that although there is a slight effect on the frequency of the longitudinal mode in the T-burner, the amplitude of each order of oscillation increases more significantly with the increase of pulse charge. According to Figure 9(b), the pressure oscillations are dominated by the first and second order with the pulse charge of 0.1g- 0.2g. With the increase of pulse charge, the higher order signals in the pressure oscillation also be enhanced. Besides, the FFT results at a higher frequency range were also analysed. The peak frequencies of the FFT curves were plotted in Fig. 10 and compared with the theoretical frequencies of the acoustic modes. The results show that the peak frequencies of the amplitude-frequency characteristics are in great agreement with the theoretical tangential frequencies, which confirms the existence of tangential oscillations mentioned in section 3.1.

DOI: 10.13009/EUCASS2023-474

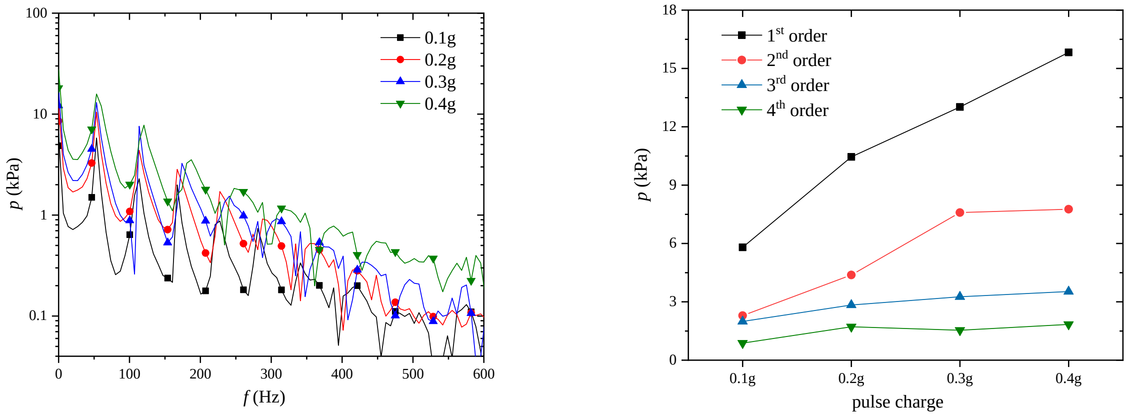

(a) The FFT results (b) The amplitude of different orders

Figure 9: The amplitude-frequency characteristics under different pulse charges

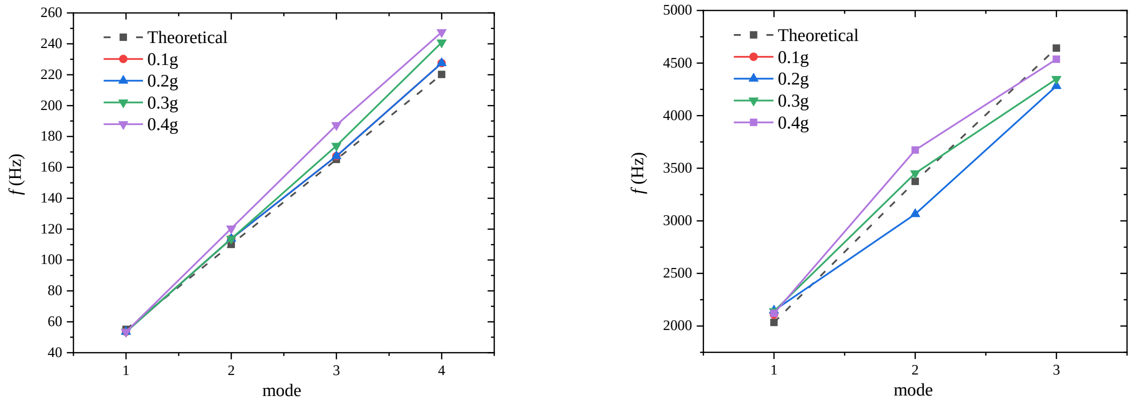

(a) Longitudinal modes (b) Transverse modes

Figure 10: The oscillation frequencies under different pulse charge

The calculation of the attenuation constants with different pulse charges are plotted in Figure 11. The results show that the test with high pulse charge present larger attenuation constants than test with low pulse charge, which indicates that the attenuation process of the pressure oscillation is more intense at high pulse charge. The pulse propagation velocities with period were also calculated for different pulse charges, as shown in Figure 12. According to the results, with the increase of pulse charge, the pulse propagation velocities at each period increase significantly. Although the pulse propagation velocities gradually decrease to the theoretical velocity of sound after several periods, the number of periods is different for each condition. At a pulse charge of 0.1g, the pulse propagation velocity decreases to near the theoretical velocity of sound after about 3 periods, while when the pulse charge increases to 0.4 g, it takes 5 periods to get close to the theoretical velocity of sound.

During the first few periods of pulse wave propagation, the discrepancy in pulse propagation velocities can be very large for different pulse charges. After the pulse wave is released for 1/2 period, the propagation velocity is 405.95 m/s at 0.1 g, but reaches 521.74 m/s at 0.4 g pulse charge. This further confirms that the pressure oscillations in the T-burner during the first few cycles after pulse release exhibit the characteristic of typical of travelling waves. The pressure oscillations in the T-burner during above process are significantly influenced by the pulse charge. Therefore, the measurement of the pressure coupling response using the T-burner requires an analysis focusing on the validity of the data within the first few cycles. The higher the pulse charge, the longer it takes for the pulse propagation velocities to decrease to the velocity of sound. The pulse charge should be kept as low as possible to minimize the effect on the test results of the pressure coupled response function.

DOI: 10.13009/EUCASS2023-474

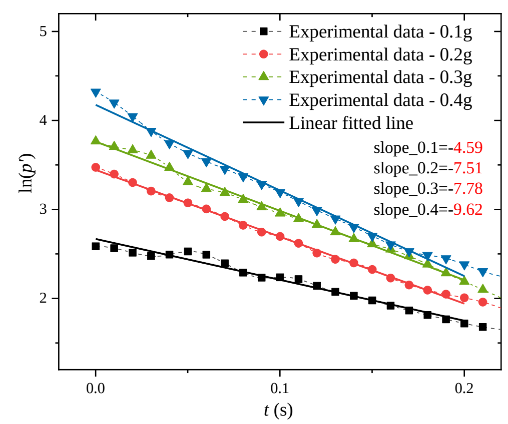

Fig.11 The attenuation constants under different pulse charges

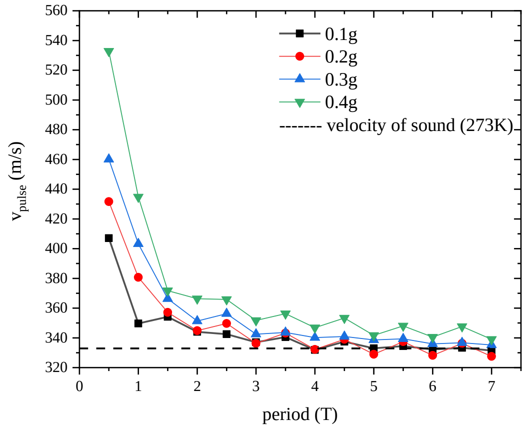

Fig.12 The pulse propagation velocities with period under different pulse charges

3.3 The effects of the chamber pressure on pressure oscillation

In order to investigate the effect of the chamber pressure on the pressure oscillation characteristics, the chamber pressure was changed from 0 MPa to 2 MPa in tests 5-7. The pressure oscillation curves were shown in Figure 13. The results show that the pulse wave front is steeper and the compression degree is enhanced with the increase of combustion chamber pressure. Both of the first pulse δp and the increase rate of the pressure $\delta p/\delta t$ are increase with the chamber pressure, but the values for the atmospheric pressure condition are much smaller than those for the high-pressure conditions. This is due to the compression from the external chamber pressure to the pulser, resulting in a higher pulse wave energy density as the pulse excitation needs to reach a higher pressure to break through the seal filler.

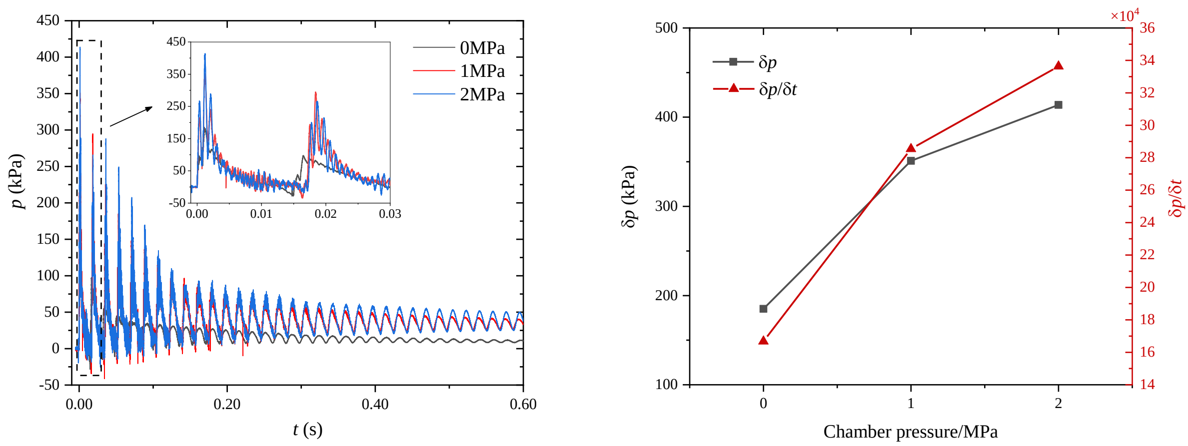

(a) The pressure oscillation curves

(b) δp and $\delta p/\delta t$ with different chamber pressure

Figure 13: The pressure signals under different chamber pressure

FFT analyses were carried out on the pressure signals in the time range of 0 to 0.5 s to obtain the amplitude-frequency characteristics of the longitudinal oscillation at different chamber pressure, as shown in Figure 14. The results show that the amplitude of each order of oscillation increases significantly with the increase of chamber pressure, indicating that the energy density of the pulse wave increase when the combustion chamber is under higher pressure. At the same time, the energy distribution of each order for different chamber pressures is not uniform, and the energy transfer mechanism between different orders needs to be further investigated.

DOI: 10.13009/EUCASS2023-474

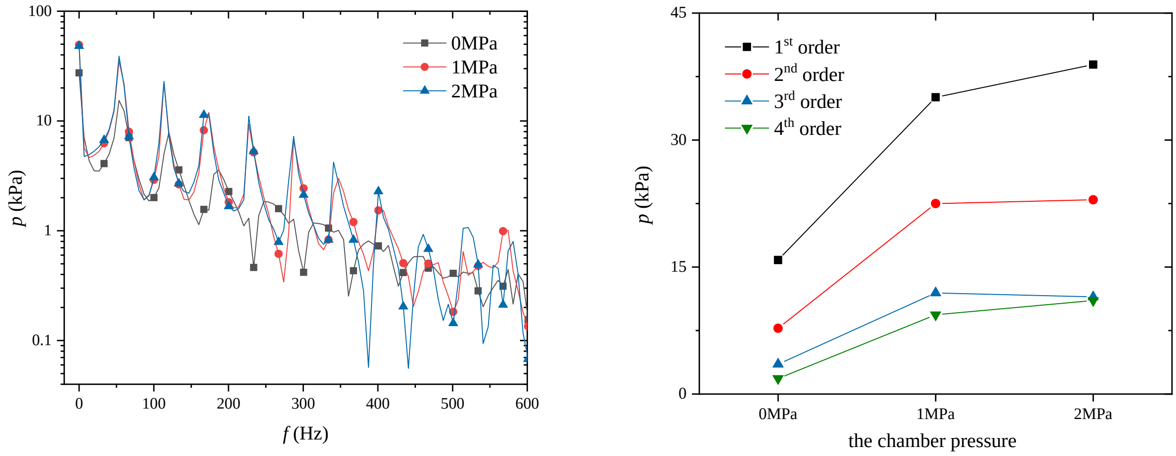

(a) The FFT results (b) The amplitude of different orders

Figure 14: The amplitude-frequency characteristics under different chamber pressure

Figure 15 shows the calculation of the attenuation constants of pressure oscillations with different chamber pressure. The results show that the attenuation coefficient decreases with increasing combustion chamber pressure, which is due to the larger damping in the chamber under high-condition, resulting in a slower attenuation of the pressure oscillation. Figure 16 shows the pulse propagation velocities with period under different chamber pressure. According to the results, due to the compression from the external chamber pressure to the pulser, the pulse propagation velocities decrease significantly with the increase of chamber pressure. It can also be seen that the pulse propagation velocity in the pressurized condition decreases rapidly from about 400 m/s to 350 m/s within 3 cycles, and the decreasing trend of the pulse propagation velocities is much slower in the high-pressure condition. This suggests that although the initial velocity of the pulse is relatively lower in the high-pressure case (considered close to the velocity of sound in the literature [2]), it takes longer for the pulse propagation velocities to decrease to the velocity of sound. The conversion of the pulse waveform from traveling waves to standing waves is even slower. Therefore, the effect of waveform conversion under different pressure needs to be considered during the measurement of the pressure coupling response function using the pulsed T-burner.

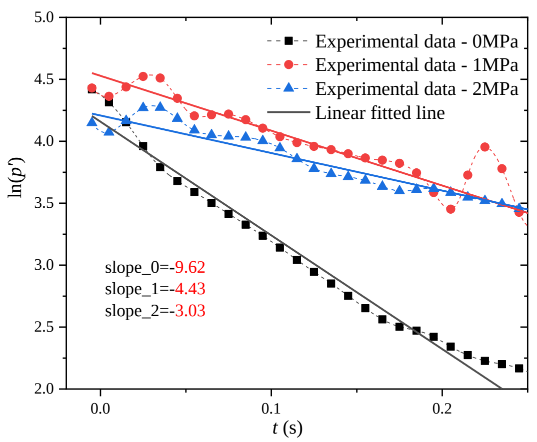

Fig.15 The attenuation constants under different chamber pressure

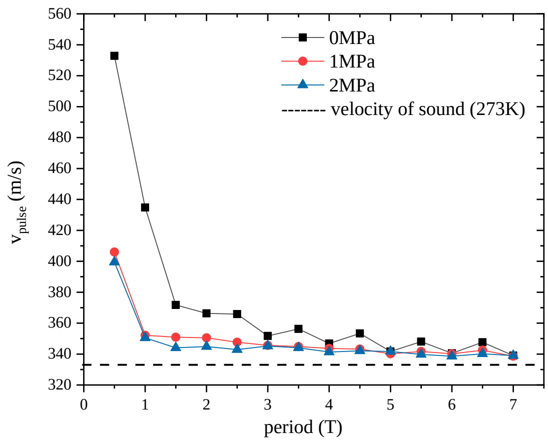

Fig.16 The pulse propagation velocities with period under different chamber pressure

4. Conclusion

In this paper, a pulse ignition system based on T-burner was designed to measure the pressure oscillation in chamber. We explored the amplitude-frequency characteristics of pressure oscillation after a pulse triggering. The oscillation waveform, pulse wave propagation speed and pulse wave attenuation constant were also investigated under different pulse charge and chamber pressure respectively. The results showed that there is a conversion process in pulsed waveform from travelling waves to standing waves, which takes several periods. This is the reason for the great

DOI: 10.13009/EUCASS2023-474

uncertainty in the results of pressure coupling response measurements using pulsed T-burners, as the typical traveling wave state present in the combustion chamber is not usually taken into account in data processing for the test results at present. With the increase of pulse charge and chamber pressure, the amplitude of pressure oscillation, oscillation frequency and attenuation coefficient all increase, while the propagation velocities of pulse wave gradually slow down. The higher the pulse charge and chamber pressure, the longer it takes for the pulse propagation velocities to decrease to the velocity of sound. Therefore, the effect of waveform conversion under different conditions needs to be considered during the measurement of the pressure coupling response function.

Compared to the past researches, the present work focused on identifying the validity of the pulse to trigger instability. The influence of the powder charge and chamber pressure on pressure oscillation indicates that the effects of the pulse can be predicted by controlling the external condition, and is potentially useful for motor designers to evaluate the stability margin of motor. However, the tests were only carried out in the T-burner and the effect of structure was not considered. Future work should therefore include considering the influence on the lengths of chamber. More tests should be carried out in full-scale rocket motors.

References

[1] R. L.Glick. 1980. Pressure-Coupled Response of Composite Solid Propellants. Journal of Propulsion and Power, 19:406-408.

[2] Yan M, Wang N, Li J, et al. 2017. Experimental and theoretical study on characteristics of pulse excitation in T-burners. Acta Astronautica. 134: 278-290.

[3] F. E. C. Culick. 2006. Unsteady motions in combustion chambers for propulsion systems. Technical report, AGARDograph, NATO/RTO-AG-AVT-039.

[4] Su W, Wang N, Li J, et al. 2014. Improved method of measuring pressure coupled response for composite solid propellants. Journal of Sound and Vibration. 333(8): 2226-2240.

[5] J. D. Baum, J. N. Levine. 1986. Modeling of nonlinear longitudinal instability in solid rocket motors. Acta Astronautica. 13(6): 339-348.

[6] Kaplan E, Yazıcı B, Ak M A, et al. 2009. Experimental study of a T-burner resonator. International Journal of Energetic Materials and Chemical Propulsion. 8(3): 173-182.

[7] Gallier S, Briquet B, Yiao M. 2019. Aluminum Combustion Can Drive Instabilities in Solid Rocket Motors: T-Burner Study. Journal of Propulsion and Power. 35(1): 159-172.

[8] Genot A, Gallier S, Schuller T. 2019. Model for Acoustic Induced Aluminum Combustion Fluctuations in Solid Rocket Motors. Journal of Propulsion and Power. 35(4): 720-735.

[9] Rock S G, Habchi S D. 1997.Advanced Computational Model for Rocket Plume Effects on Escape Systems Aerodynamic Characteristics. CFD Research Corporation.

[10] R.L. Coates, N.S. Cohen, L.R. Harvill. 1967. An interpretation of L' combustion instability in terms of acoustic instability theory. AIAA Journal. 5:1097-1102.

[11] Qiao, Z. 2011. Research on Oscillation Characteristics Induced by Vortex Acoustic Coupling in Solid Rocket Motors. PhD Thesis. Beijing Institute of Technology, School of Aerospace Engineering.